Detailed Description of the Molecular Organization behind AFM Images of Polymer Coatings: a Molecular Modeling Approach

David Zanuy,[*a] Georgina Fabregat,[a,b‡] Jordi Triguero[a] and Carlos Alemán[*a,b]

[a] Departament d'Enginyeria Química, Campus Diagonal Besòs, c/Eduard Maristany, 10-14, Edifici I, Planta 2, 08019 Barcelona

[b] Barcelona Research Center in Multiscale Science and Engineering, C/ Eduard Maristany, 10-14, Edifici I, Planta S, 08019, Barcelona

[‡]All experimental work has been performed by GF

E-mail: david.zanuy@upc.edu and carlos.aleman@upc.edu

Abstract

The current experimental techniques of surfaces characterization provide structural information on a much larger scale than that in which atomistic details can be observed. In this work, this size gap gets reduced by consistently combining different modeling techniques that leads to describe the topographic profiles of thin polymer coatings at the atomistic level. A new modeling protocol, that combines Monte Carlo generation with Molecular Dynamics relaxation, has allowed us reproducing the experimental topography of extremely thin Poly(3,4-ethylenedioxythiophene) coating films using only the generated molecular models. The clue element of this protocol relies on parceling the studied surfaces in independent small plots, of which detailed molecular models are built. Combining a finite number of independent models enables to mimic the molecular organization of a large length of film that is orders of magnitude lager than the commonly used size in molecular models. The reconstructed area reproduces the thickness and roughness of very thin polymer coatings that were explicitly obtained for this study using very short electropolymerization times. This work shows a feasible way of visualizing with atomistic detail coated surfaces with polymeric films.

Introduction

The atomistic details of polymer based materials are seldom available from microscopic observations. Most of the experimental techniques used to characterize the topographic features roughly encompass scales that reach decimals of micrometers. These technical limitations are generally ignored and most of the available literature about the atomistic organization of polymeric materials shows structures that are fitted to low resolution images based on known systems without much attention to their actual feasibility.[1] Yet, most available structural works are completed without assessing the basic details of those systems, generally by either avoiding the atomistic nature of the polymer ensembles with simplified coarse-grained models,[2] models that do not properly described the system energy,[2] or by totally ignoring the atomic organization approaching the problem to finite elements computations.[3] Beyond these simulation limitations, experimental techniques are not generally tuned for the atomistic description of the polymer bulk, lacking the required structural finesse. Atomic Force Microscopy (AFM) and other more classic electronic microscopy techniques do not provide yet such details on polymers ultrastructure. We believe that these methodologic limitations can be overcome by strategically combining the available mathematical algorithms with Force Fields calculations. In this work, a novel modeling strategy is presented for obtaining a fast and reliable atomistic description of a grafting polymer using molecular models based on classical mechanics. Our results are validated by comparing experimental topographic magnitudes obtained on the actual polymer films deposited on metal surfaces.

Metal surfaces coated by polymers are commonly found in nowadays literature for micro-engineering applications, because this sort of nanoscale constructs is especially

suited for electronic micro-circuitry. Reduced scale circuitry requires the use of low density materials that can efficiently store and release charge. Electroactive Conducting Polymers (ECPs) are an excellent choice for becoming important building blocks on nanocircuitry.[4] ECP are stable macromolecular scaffolds that show induced and reversible electrochemical activity, which is a direct consequence of allowing several oxidation states. They show as well simplicity and versatility of synthesis (e.g. chemical synthesis, vapor-phase oxidation and electrochemical processes) and satisfactory environmental stability. Poly(3,4-ethylenedioxythiophene), abbreviated PEDOT, features the majority of those properties: excellent conductivity (up to 500 $S \cdot cm^{-1}$), optimal environmental and chemical stability, fast doping–dedoping processes and exceptional biocompatibility.[5,6] Moreover, PEDOT shows excellent electroactivity and electrostability, both explaining its high ability to reversibly exchange charge.[6-9] These features makes PEDOT suited for its inclusion as active parts in both rechargeable a batteries and electrochemical ultracapacitors.[9-12] Symmetric ultracapacitors including very thin PEDOT films (i.e. those with a thickness, ℓ, typically lower than 250 nm) are among the most reliable choices, due to their excellent capacitive properties.[13-15] This work investigates the ultrastructure of coated metal surfaces that were designed for working as capacitor electrodes.[13-15]

Although PEDOT on steel constructs have extensively been examined by both scanning electron microscopy (SEM) and AFM,[13-15] structural details about its deposition and growth are yet very scarce. Molecular simulation approaches recently hinted few defining features of these nano-constructs never proven before.[16] Our initial attempt to represent the molecular details of the polymer bulk failed to describe the surface properties (e.g. topography and morphology), because we relied on polymer chains of

unique lengths, relinquishing to explore the roughness of the polymer coated surface. Unfortunately, surface roughness is one of the ions movement determinant during oxidation and reduction cycles, i.e., explains how topography affects the charge exchange in these systems.[13-15,17]

The results presented in this work represent a significant improvement with respect our initial approach that has allowed us overcoming previous limitations, whereas we kept reducing the gap between the experimental scales in which surfaces are studied and the feasible use of force field based techniques within reasonable computation times. Therefore, we demonstrate the reliability of our approach by exploring with AFM the topography of newly synthesized PEDOT on steel electrodes using extremely short polymerization times (symbolized by the Greek letter θ), $\theta \leq 5$ seconds, and comparing the surface topographies with the roughness computed using our atomistic modeling that combined stochastic generation with molecular dynamics energy relaxation.

Methods

Experimental techniques

Materials.

3,4-Ethylenedioxythiophene (EDOT) and acetonitrile of analytical reagent grade were purchased from Aldrich. Anhydrous LiClO4, analytical reagent grade, from Aldrich was stored in an oven at 80°C before use in the electrochemical trials.

Polymerization.

Poly(3,4-ethylenedioxythiophene) (PEDOT) was polymerized by chronoamperometry (CA) under a constant potential of 1.40 V. All the anodic electropolymerizations and electrochemical experiments conducted in a three-electrode two-compartment cell under nitrogen atmosphere (99.995% in purity) at 25°C. The anodic compartment was filled with 40 ml of a 10 mM EDOT solution in acetonitrile containing 0.1 M $LiClO_4$ as supporting electrolyte, while the cathodic compartment was filled with 10 ml of the same electrolyte solution. Steel AISI 316 L of 1×1 cm^2 was employed as working and counter electrodes. The reference electrode was an Ag | AgCl electrode containing a KCl saturated aqueous solution (E^o=0.222 V at 25°C), which was connected to the working compartment through a salt bridge containing the electrolyte solution.

Atomic force microscopy (AFM).

Topographic AFM images were obtained with an AFM Dimension 3100 microscope using a NanoScope IV controller under ambient conditions, in tapping mode. A silicon TAP 150-G probe was used (resonant frequency and force constant of 150 kHz and 5 N/m, respectively). AFM measurements were performed on various parts of the films,

which produced reproducible images similar to those displayed in this work. The scan window sizes used in this work were 5 × 5 and 2 × 2 μm^2.

Stylus profilometry.

The thickness (ℓ) of the films was determined through profilometry measurements using a profilometer Dektack 6 from Veeco. Imaging of the films was conducted using the following optimized settings: stylus force 1.5 mg and speed 15 nm/s.

Computational methods

Generation of Starting Models.

All atomistic models were built using an in house program. Our stochastic growth algorithm was recently introduced in reference 18. In this work, 60 identical PEDOT chains (made of different number of EDOT repeat units each one) were used to emulate the polymer deposition on a metallic substrate, following the approaches already described in previous works.[16,18] Before starting the growth cycles, PEDOT chains were arranged fully extended, represented as rigid conformers, oriented parallel to z-axis and were randomly distributed on the iron atoms surface. The only restriction imposed to their distribution over the steel surface (i.e. their equatorial projection on the surface plane) was to minimize the steric hindrance between neighboring chains. Lennard-Jones potential adapted to AMBER force field was used to achieve this goal.[16,18,19]

In order to represent the asymmetric growth, sets of chains are randomly selected and make them grow by adding a random number of EDOT repeating units. At each simulation cycle, *i* new structures are built and only one will be selected. Every new structure shares with the other new ones the total amount of repeats that will have been

added, amount that had been randomly selected before a new cycle started. After selecting how many RUs are going to be added, a number of chains are selected for each new structure to be built. This number of nascent chains is also randomly selected within a previously set margin. In the presented set of simulations this margin was from 1 to 10 (previous trials showed that was a good compromise between acceptance probability and generation speed). Per each chain, the number RUs that will be added is also selected randomly. Although the total number of added RUs is the same for each new built structure, the number of chains that grow and the increment on RUs per chain is totally different. In summary, each cycle generates *i* structures, each of them comes from adding $n=n_1+n_2+\ldots n_m$ repeats to *m* chains. Each structure has a different number *m* growing chains and a different combination of n_m repeats per chain.

Each of these new structures will suffer an energy change that will be computed to ascertain the thermodynamic probability of acceptance for every introduced change. Our program uses a modified Metropolis criterion, analogous to that used in the ConRot method,[20] in which the acceptance probability is not directly assessed by the energy difference of the starting and final point but by computing the probability of each individual change: if the chain *m* grows n_m RUs, per each new n_m repeat units placed in chain *m*, a thermodynamic probability is computed as:

$$W_{n_m} = \frac{e^{-\beta \varepsilon_k}}{\sum_{k=1}^{n_m} e^{-\beta \varepsilon_k}}$$

Where n_m is the number added new RUs, W_{n_m} is the probability weight of each combination of added RUs and β is $(T\kappa)^{-1}$, where T is Temperature in K and κ the Boltzmann constant.

The final probability of accepting a structure will be the product of all the $m \times n$ individual probabilities.

$$W_{built\ model} = \prod_{m} W_i$$

Each cycle finishes when one of the new model fulfills the modified Monte Carlo criterion:[18]

$$P_{acc} = \min\left(1, \frac{P_i W_{i+1}}{P_{i+1} W_i}\right)$$

It is very important not to misunderstand the meaning of this generation method: our procedure does not try to reproduce the growth mechanism of PEDOT but to build reliable atomistic models to represent the surface morphology once all the modeling stages are finished. Counterions (dopant agents) are placed along the new EDOT units in positions that reproduce the organization previously observed.[18] An example of a finished model can be seen at **Figure 2**, left panel.

Energy Relaxation.

Models derived from the deposition and growth algorithms are rigid and do not take into account the effect of temperature and pressure. Thus, before characterizing the topology and topography, energy optimization and MD trajectories were run for all generated models. Each model is contained in an orthorhombic cell of 7.665nm × 7.665nm × "*c*", in which the space not occupied by the substrate and polymer is filled with solvent molecules (acetonitrile in this case[16]). Depending on the total amount of RUs present in each generated model (later referred as *micromodel*) different amount of acetonitrile molecules was required to ensure the correct periodical conditions under the

used cutoff (see below). Hence the chemical composition of each set of micromodels was equalized both in number of RUs and solvent composition, ranging from 7358 molecules of acetonitrile for 17200 RUs models to 10746 molecules in those that presented 28000 RUs.

Force Field details for MD.

All parameters were extrapolated from AMBER03 libraries[21] with exception of partial charges of the EDOT repeating unit, which had previously been parametrized[19,22], and ClO_4^- parameters that were obtained from Baaden et al., 2000.[23] Bond and length distances of PEDOT repeat units were approximately kept at their equilibrium distances using the same strategy employed at reference 22. Steel surface was represented as an iron crystal organized following an FCC lattice, as it was discussed in reference 16. Periodic boundary conditions were applied using the nearest image convention and atom pair cut-off distance was set at 14.0 Å to compute the van der Waals interactions. In order to avoid discontinuities in the potential energy function, non-bonding energy terms were forced to slowly converge to zero, by applying a smoothing factor from a distance of 12.0 Å. Beyond cut off distance, electrostatic interactions were calculated by using Particle Mesh of Ewald, with a points grid density of the reciprocal space of $1Å^3$.[24]

Molecular Dynamics: Simulation details.

All simulations were performed using the NAMD 2.9 program.[25] Each system was submitted to 5000 steps of energy minimization (Newton Raphson method) and this was the starting point of several mini-cycles of optimization and equilibration. The

numerical integration step for all runs was set at 1 fs and the non-bonded pair list was updated every 1000 steps (1 ps).

The following protocol was applied to all 1170 studied models. Solvent phase was first equilibrated. 10^5 steps of heating and equilibration at NVT conditions were run to stabilize the solvent phase at 298K. The Berendesen thermostat was used[26] with a relaxation time of 1 ps. Then, the solvent density was equalized to its optimum value using $2.5 \cdot 10^5$ steps of NPT simulation at 298 K. The Nose–Hoover[27] piston combined with the piston fluctuation control of temperature implemented for Langevin Dynamics[28] was used in the late cycle. Pressure was kept at 1.01325 bars, the oscillation period was set at 1 ps while the piston decay time was set at 0.001 ps. The piston temperature was set at the same value as the thermostat control, 298K, which used a damping coefficient of 2 ps. During these couple of cycles, all solid phase atoms were kept frozen (iron, polymer and counterions).

Once the simulation box dimensions were stabilized, the final equilibration cycles would begin. After unfreezing the rest of atoms (solid phase with exception of the iron atoms[16]), $2 \cdot 10^5$ steps of NVT simulation were performed to thermally equilibrate the whole biphasic system. For the latter run the Langevin method[29] was used to maintain the system temperature constant with a damping coefficient of 2 ps. Finally, 1.0·106 steps of anisotropic pressure control (NPzT conditions) were run to reach the required simulation conditions. In the NPzT ensemble, only the box length in the z-direction is allowed to change, where the z-component of the pressure tensor is equal to the external pressure.[30] The last snapshot of the anisotropic equilibration was the starting point of 2

ns of production time. The production runs were all performed under the same conditions previously mentioned for the NPzT equilibration.

Computations of the topographic magnitudes

Thickness (ℓ).

Thickness was computed per each of the generated micromodels (see text) as the absolute average of each present chain deposited over the metallic surface.

Roughness (R_a and R_q).

The arithmetic average height (R_a) and the root mean square roughness (R_q) where computed for each of the generated micromodels using the following expressions[31]:

$$R_a = \frac{1}{n}\sum_{i=1}^{n}|y_i| \quad (1)$$

$$R_q = \sqrt{\frac{1}{n}\sum_{i=1}^{n} {y_i}^2} \quad (2)$$

Where y_i is the distance from the top of a peak to the average line (as the average height of the 60 explicit chains) or the distance from the bottom of a valley to the same average line, and n represent the number of studied peaks or ridges.

Results and discussion

Topography of the polymer coated surface

In order to reduce the size of the structure to be modeled, we used very short polymerization times, which led to an unknown scenario, because of the uncomplete cover of the metallic surface. Under such conditions, the previously observed homogeneity of PEDOT polymer films is lost. **Figure 1** shows selected AFM images for several samples of PEDOT polymerized at both θ= 1s and θ= 3s. Inspection to **Figure 1a** confirms that the polymer coating is not completed after such short time periods, which is further manifested by higher dispersion of polymer thickness (see below). Evidently, **Figure 1** also manifests that the larger is the polymerization time the more extensive is the morphologic homogeneity, showing much regular dispersion when θ is 3s than when is 1s (**Figure 1b** compared with the former). Nonetheless, a more detailed examination of those regions that have already been covered by polymer at θ= 1s show several features yet observed in cases in which polymerization was completed:[32] PEDOT chains tend to organize in a dense distribution of sharp peaks forming two differentiated levels. On the top level, very small number of high and compact clusters forms from aggregation of peaks, whereas the bottom level involves individual peaks and low clusters of reduced dimensions, which can be associated to most recent formed polymer chains that accumulate at the bottom of the valleys. A closer inspection to these regions reveals considerably thicker polymer coatings than could be expected. Moreover, increasing θ apparently only improves the coating uniformity of the metallic surface but not its thickness.

A summary of the measured thickness (ℓ) and roughness (R_q and R_a)[31] per each studied case is presented in **Table 1**. A detailed collection of both thickness and roughness measurements is presented in the *supplementary information*. The averaged ℓ values observed in the studied PEDOT films ranged from 173±49 to 256±80 nm, respectively after θ = 1 and 3 s of polymerization (**Table 1**). These values are in general agreement with previous works in which polymerization times were long enough to completely cover the metal surface.[32] As mentioned earlier, there are important differences. First of all, greater data dispersion is observed, in agreement with an incomplete deposition of polymer mass. Hence, the standard deviations of the measured thicknesses after θ = 1 and 3s represent 28% and 31% respectively, of the actual measured magnitude. If such dispersion is combined with the values reported in previous works,[12-15,18] a new scenario emerges: there is always a rapid polymerization, in less than a second, that leads to the formation of significantly long polymer chains. At the same time, those early growing chains quickly and irregularly settle over the metallic surface. By contrast, at longer θ part of the deposition must be related to refilling of the aforementioned low clusters, those initially created cavities in between high peaks. This idea is strengthened by how thickness varies as function of polymerization time. A threefold increment in the polymerization time does not lead to a thickness enlargement of that order but only of 1.5 times. An increase of 10 times in polymerization times only provides two times thickness enlargement.

Roughness, determined as both root mean square (R_q) and mean average (R_a) of the deviation of the sample high from the mean line over the sampling length, shows very similar trends. None of both magnitudes follow a linear correlation

with respect to θ increments, being the differences in roughness with respect to polymerization time even smaller than those observed for thickness. Visual inspection to the organization of PEDOT films shows polymer layers that feature a profoundly rugged surface, with deep valleys surrounded by significantly high peaks, as can be observed in **Figure 1b** that compares the 3D roughness profiles for samples obtained at both studied θ's. Again, the reduction on the surface roughness when polymerization time increases is noticeable at first sight, clearly pointing towards the same idea introduced above: first chains of minimal length get deposited on the surface leaving pronounced valleys, partially unoccupied spaces, which at larger θ's are refilled by newly polymerized chains. Thus, the thickness increment is much higher than the increment in roughness from θ= 1s to θ= 3s.

Table 1. Thickness (ℓ, in nm), roughness (R_a and R_q, in nm) measured by AFM for PEDOT films deposited on steel substrate using different polymerization times (θ, in s). Values are obtained over 5 samples per each θ.

Polymerization time (θ)	**ℓ[a]**	**Roughness[b]**	
		R_q[c]	R_a[c]
1	173±49	45±14	37±13
3	256±80	61±6	48±5
10*	350±10	117±3	94 ±7

[a] Measured by ASH profilometry. [b] Measured by AFM. [c]RMS and average roughness (R_q and R_a, respectively). *Data extracted from reference 32, for context and comparison with smaller θ shown in this work.

The averaged value of roughness reveals that multiplying by 3 and by 10 the polymerization time, only implies a roughness enhancement of factors of 1.3 and 2.6, respectively (**Table 1**). Moreover, even the data dispersion of roughness

measurements decreases when the polymerization period increases. While the standard deviation of thickness increased 63% when the θ is triplicated, roughness dispersion dramatically drops to values that are 130% lower when going from θ =1s to θ =3s. This correlation between smoother topography and larger polymerization times was already characterized in PEDOT films but using much longer polymerization times (i.e. from 10 to 300 s).[12] This effect is significantly more pronounced in the PEDOT films studied in this work, which are much thinner due to shorter θ, and again points towards the aforementioned new mechanistic interpretation. If larger θ implies smaller roughness dispersion, it necessary means that at certain time frame, between θ=1s and θ= 10s, the new polymerized segments preferably fill the gaps left in early generation steps rather than contribute to enlarge existing polymer chains. Thus, the longer is θ the larger the polymer baseline will become (i.e. both observed thickness and roughness).

Modeling Polymer Roughness: Reducing dimensions of system to increase feasibility

Modeling the ultrastructure of a macromolecular assembly and doing it in a size scale comparable to that of the experimental methods is still a challenge of complex solution. Commonly, computational chemists rely on coarse graining models to face this complexity and sizes.[33-34] Yet, the information provided by these approaches is very dependent on the molecular templates used to parametrize not only the magnitudes that define the inter-molecular relationships but also the mathematic expressions used to compute them. This limitation affects the structural and physical features that can be characterized at length scales between the μm and the nm. Within this context, we decided to face these

limitations trying to achieve the nm scale by reducing the scale of at least two of the three space dimensions, which made possible to obtain polymer assemblies of chain lengths closer to the μm scale than to the nanometer scale. In order to achieve this goal we adapted a previously develop strategy[16] to simulate the outcome of polymer growth.[18] It is important to clarify that our methodology does not pretend to model the polymerization reaction, neither its kinetics nor its reaction mechanism. We developed a simple and effective strategy that generates polymer assemblies with consistent intermolecular organization.

Trying to comprise the mesoscopic organization on the surface shown in **Figure 1b** at once is still an impossible mission by all means. However, the observed structural disposition allows some degree of simplification. Most of the topographic features of these coated surfaces are the consequence of an asymmetric disposition of the polymeric material. There is a consistent scale misalignment between the extension of the metal surface covered by polymer chains (and their lateral organization) and their vertical growth. In other words, the topographic exploration is performed over the μm scale (pictures shown in **Figure 1b** represent surfaces of 4 μm^2) whereas the vertical scale is within an acceptable range for atomistic models, especially in cases corresponding to polymerization times of 1s. This quick polymerization leads to thickness and roughness in the order of hundreds nm, which is right on the feasibility of atomistic constructs. Thus, the classic strategy of divide and conquer can be applied to our problem.

We reduce most of the system complexity to a small set of variables to be optimized onto the growing direction, which is coincident with the vertical one,

as we previously showed.[16, 35] Hence, the lateral organization of polymer chains and their vertical growth are initially modelled disregarding the macro-organization over the metallic surface and we focus our efforts on reproducing both thickness and roughness. In order to achieve this goal the equatorial superficial projection for our molecular model is reduced to a minimal expression (7.665×7.665 nm^2) whereas the vertical extend of polymer chains is only limited by the total numbers of repeating units (*RUs*) to be added onto a fixed set of nascent chains, number previously fixed to maintain the amount of polymer mass per unit of area. The only variable that will be modified in order to keep constant the density of the polymer bulk is the vertical "addition" of EDOT RUs. Before moving forward on our modelling results, we summarize the main approaches on which our in house code was based.

In order to expedite the generation of atomistic models, rigid geometry was assumed for the polymer molecules. All molecules present their molecular geometries at the equilibrium values during the polymer coating generation. The energy of the system only includes non-bonding terms, with Van der Waals energy represented by a Lennard – Jonnes potential and the electrostatic energy by the untruncated Coulomb potential. The averaged degree of oxidation per EDOT RUs had already been determined to be +0.5 charge units, under the experimental conditions used in PEDOT electropolymerization.[36] A counter-ion (perchlorate molecular anion) is added per each pair of EDOT units included in the molecular model. Thus, when our computational algorithm starts making the nascent chains grow the acceptance criterion guarantees generating assemblies without neither high steric hindrance nor electrostatic repulsions.

Before this work, we could only demonstrated that PEDOT chains laterally associated with the perchlorate anions acting as cement via electrostatic attraction between oppositely charged centers, whereas they shielded the inherent repulsion between positively charged EDOT units.[16] However, we could not correlate topography with molecular structure, mainly because our modelling algorithm dealt with very short polymer chains (10 nm), and furthermore, all those chains had the same number of repeating units, making models totally flat without roughness. In order to overcome this shortcoming, without saturating the generation of new models, we focused on elongating polymer chains that had been previously distributed in very small areas. Thus, if experimental samples extended over surfaces of 2×2 μm^2, we generated a representative number of independent models, on per each starting distribution of 60 chains over the selected steel area (7.665 × 7.665 nm^2). Details about how to choose a representative number of atomistic models are provided below for each studied topographic feature. Thus, each atomistic model based on the aforementioned surface plotting will be further referred as *micromodel* (see **Figure 2**, Top panel, *rigid model*).

The generation of any micromodel is finished when a targeted total amount of RUs is reached, i.e., when the summation of the RUs that each nascent chains initially present plus the number RUs incorporated during the growth procedure reaches that targeted RUs number. In order to reach an atomistic representation of the experimental size (lateral length of one of the surface directions) a single molecular model can be built by laterally combining all generated micromodels

(see below for practical details). All models are uncorrelated by definition and all of them are local energy minima respect the non-bonding potentials. This strategy is faster and more efficient than trying to cover a $4 \cdot 10^6$ nm^2 of alloy with 60000 chains of polymer and then simulate their growth, which includes also adding a perchlorate anion per every two new EDOT RUs. Such simulation would imply computing millions of non-bonding pairs per each generation cycle (addition of new RUs), making the model production totally unfeasible in terms of both computing time and memory demands. Our divide and conquer idea allows to produce in just few hours micromodels with chain lengths in the order of the μm scale (vertical growth). Each micro-model implies the computation of only few hundred thousands of non-bonding pairs per cycle, which is totally affordable with the contemporary computational power.

What conditions the final topography?

Despite the simplicity of our rational there are several questions that are not straightforward. We knew thickness should be the average high of the shortest chains present in the systems whereas roughness should be a reflection of the dispersion of chain lengths. Therefore, we first assessed what was the minimal amount of independent models required for reproducing the experimental thickness. As stated above, this feature depends on the average high of the shortest chains. Within our molecular production scheme is equivalent to ascertain how many RUs are incorporated to each micromodel once the production run is finished. At this point, we needed to produce enough micromodels to make the computed data representative but we did not require yet to reproduce the whole extend of the experimentally studied surface length. If the

simulated surface were within the averaged horizontal length of observed peaks, the thickness information would be statistically demonstrative. The average length of most peaks depicted in **Figure 1c** is 0.196 μm, which is approximately 26 times the horizontal length that was set to define the deposition surface of each micromodel.

Table 2. Average computed value of thickness depending on the total number of EDOT RUs used per each set of micromodels (left column) and the initial length of the nascent chains (length expressed as number of RUs per polymer chain).

Total number of RUs	**Initial number of RUs per polymer chain**					
	2	**20**	**40**	**60**	**120**	**$<\ell>^a$**
17200	110.5	110.8	110.9	110.9	110.9	110.8±0.2
18000	116.1	115.9	116.1	116.2	116.2	116.1±0.1
20000	128.8	128.9	129.1	129.0	129.2	129.0±0.2
22000	141.9	141.9	142.1	142.0	142.1	142.0±0.1
24000	154.8	154.7	154.8	154.8	154.9	154.8±0.1
26000	167.9	167.7	167.9	167.9	168.0	167.9±0.1
28000	180.4	180.2	180.4	180.6	180.5	180.4±0.2

[a] averaged thickness over the 5 different starting points per each set of 26 micromodels with the same final amount of RUs. As mentioned in the text each micromodels consisted of 60 polymer chains randomly distributed over 58.75 nm^2. All presented values are presented in nm.

As it was introduced earlier, each microscopic model presents only 7.665 nm of lateral length in both x and y directions. In order to have an acceptable atomistic representation, we will rely on sets of 26 independent micromodels to compute thickness per each presented case. In other words, each studied case will constituted by 26 independent microscopic distributions of 60 independent nascent chains over a metallic surface of 7.665 × 7.665 nm2 (**Figure 2**, *middle panel*). These 26 micromodels will only share two molecular features, the initial number RUs that the nascent chains presented at the beginning of the "growth

simulation" and the total amount of EDOT RUs that each micromodels presents once the Monte Carlo procedure has finished. Lateral association of the 26 independent microscopic models will represent the average length of the actual observed peaks. It is important to remark that the macromodel will be built by single micromodel addition at the time. Every new micromodel laterally added will then be energetically relaxed (repeating this step 25 times in this case and 259 in larger models. See below). Because we had built each micromodel with Periodic Boundary Conditions, the steric hindrance generated in the border zones of the structures placed in contact will be easily relaxed with energy minimizations.

However, there is not clear experimental evidence neither previous simulation that could convey what structural features will be reflected in the numerical value of the computed polymer thickness. Both, the length of the polymer chains that initially were deposited (or what we call in this work the *length of nascent chains*) and the random incorporation of new RUs onto those nascent chains are potential structural descriptors of this nanometric magnitude. In order to address this matter, multiple combinations of those two variables were studied, 7 different targeted final RUs amounts were set, whereas per each of these RUs figures, 5 different starting chain lengths were set. If each case was to be represented by building 26 micromodels, a total 910 micromodels were built and further relaxed using MD simulations, as described in Methods section (An example of the morphological differences after relaxing can be seen in **Figure 2**, Top panel, *relaxed micromodel*).

Before getting into how PEDOT ultrastructure can be built, the actual representability of the generated macromodels was assessed. **Figure 3a** plots the radial distribution function of all inter-ring distances between EDOT units belonging to different chains, represented for each of the previously built macromodels. In the same figure the main structural information obtained from X-Ray diffraction of PEDOT films deposited on steel is included.[36,37] Despite presenting large amount of disordered segments, the computed models are able to reproduce the most relevant crystallographic features observed in deposited semicrystalline films. Among them, the characteristic reflections of the known possible orthorhombic arrangements, in which the inter-chain distances within the crystalline structure and their multiple reflections, are fairly reproduced. The distances that represent the averaged inter-chain distances along x- and y-axes, at 15.2 Å and 13.6 Å, are present as distinguishable peaks. Furthermore, the characteristic reflection that corresponds to the distance between repeat units from the same chains (around 7Å) is also systematically reproduced in our built structures. All geometrical indications point towards a successful achievement of representative models.

At this point, it is possible to continue exploring the structural features correlated with measurable magnitudes: at molecular level polymer thickness would only depend on the total amount of RUs that are placed within a confined space, as can be inferred from **Table 2**, which shows a summary of the structural features derived from all studied cases. It is remarkable that independently of the initial chain length, thickness converges at very similar values when the same total number of RUs is reached, which demonstrates both the consistency of our

stochastic approach for building models that emulate polymer growth and the validity of our divide and conquer approach. This point is verified when the average thickness is calculated over all the models that reached the same total number of RUs. Consistently, in all cases standard deviations are below 0.5% of the averaged magnitude. Finally, this particularity also shows that our generation approach is accurate enough to provide a realistic representation of the polymer chains organization at almost nanometric scale. Once the necessary degrees of freedom had been established for reaching the right thickness, we proceed to investigate what variables conditioned the roughness description.

Table 3.- Comparison of computed roughness from 6 different sets of micromodels. All values are expressed in nm and per each set the standard deviation has been included (as mentioned above, 26 micromodels per set).

# of initial RUs[a]	**R_a**	**R_q**
1200	26.4±6.3	35.3±1.5
2400	27.4±6.4	36.3±5.6
3600	30.1±5.7	40.4±7.2
7200	35.4±7.5	45.4±1.1
7800	36.7±8.7	47.1±2.3
12480	52.7±4.6	57.0±7.7
Experimental	37±13	45±14

[a] Each set differs in the initial chain lengths but all them incorporated the same amount of residues (28000, value derived from Table 2), with the experimentally obtained roughness in deposited PEDOT on stainless steel after one second of polymerization. Those models that are closer to the real polymer organization have been highlighted with a gray shade.

This second question is closely related with the topography of the polymer coated surface. How well roughness can be described using our random growth approach, in which polymer chains grow upwards into the accessible space? One of our clue assumptions was that local lateral organization of polymer chains would not directly

interfere with the final roughness of the modeled bulk polymer. If this assumption were to be incorrect, independently of the thickness our generated micromodels, we should not be able to compute an average roughness comparable to the experimental observations. In order to answer these questions, two different possibilities were explored: either only the new RUs were responsible for the observed topographic accidents or the combination of the newly added EDOT units and the preformed chains lengths were the determinants of that observable variables.

Table 3 shows the comparison between experimental values obtained at θ= 1s and the computed roughness using different starting points, after reaching the amount of EDOT units required for describing the experimental thickness. As can be clearly observed, at equal amount of final RUs in each micromodel, the key factor for comprehend the surface roughness lies on the initial length of the nascent chains. Thus, independently of the total RUs incorporated in a confined space, the topographic description of the surface seems to only depend on how large polymer chains were before beginning the deposition itself. It is remarkable that in order to reproduce the topographic profile of the studied bulky surface, each deposited chain must reach a vertical length equivalent to 130 RUs of EDOT. Therefore, the electropolymerization must be fast enough to produce polymer chains of about 60 nm even before starting its deposition over the steel surface. This statement also fits our previous observations, in which triplicating the polymerization time did not increase three times fold the thickness of the polymer coat but mainly diminished the roughness of the studied surface. This observation can be rationalized if the polymer grows fast enough and the surface coating quickly increases its thickness by the deposition of preformed PEDOT chains.

Yet, a final question remains to be answered. We reproduce the topographic features of the studied system using very small pieces of the surface but we did not show if the combination of many small pieces reproduces a whole real profile. In other words, if our divide and conquer approach is reliable, a lateral combination of enough micromodels should provide a good explanation of the experimental topography over a lateral length of 2 μm (which is the length of used on AFM experiments). Thus, in order to have sufficiently large amount of macromodels to compare with experimental perfilometries, 1300 new micromodels were stochastically generated: each model presented 60 nascent chains with 130 RUs and the generation was completed when 12480 RUs were present in each micromodel. This latter amount of microstructures corresponds to 5 different and independent profiles over 2 μm of length per each case.

Once the energy of each micromodels was relaxed, all micromodels were combined in 5 single macromodels (3244800 RUs each), following the strategy introduced earlier in which the potential energy of every newly added micromodel was in turn relaxed. **Figure 3** compares the experimental profile obtained with the topography modeled using our approach. The similarities are significantly remarkable. Our approach of microscopically divide the studied surface in small plots and further rebuild the whole surface successfully describes the main structural and morphological features of the studied polymer film deposited steel. Not only the topographic magnitudes computed are in agreement with the experimental observations but the overall shape of the topographic details that are observed at short polymerization times are reproduced once all the micromodels are arranged in lateral clusters of 260 micromodels each.

Conclusions

In this work we have shown that using an effective modeling strategy is possible to represent the atomistic details of the bulk organization in coatings constituted by polymer depositions over metal surfaces. We developed a new synergic strategy that compiles the experimental information of the topographic features of PEDOT coatings on stainless steel and makes possible to build atomistic models that reproduce the observed experimental features.

From an experimental standpoint, we reduced the size of the target polymer coating to the lesser expression by decreasing the electropolymerization to 1 s, which allowed making extremely thin coatings. The topographic features of those polymer layers are analogous to those observed after longer polymerization times and provided an excellent model system to test our modeling strategy. In order to find a feasible way to obtain a reliable microscopic description of PEDOT coatings, the studied surface is parceled into small independent plots, as many as was required to cover a specific surface direction. By reducing the size of the area to be explored at atomistic level, it was possible to implement a generation algorithm that produces rigid atomistic models of the bulk polymer over those parceled areas. This way, the vertical extend of the polymer coating can reach hundreds of nanometers, which represent the realistic scale in which the PEDOT coatings are organized.

Despite the generation process built unrelaxed structures, their structures are close enough to achieve a realistic description, as relaxation of geometry constrictions is easily achieved using a combination of energy minimization and

short runs of Molecular Dynamics simulations. The reliability of the relaxed models is not only demonstrated when they can provide accurate values for magnitudes used to describe the topography of surfaces but by providing correct description of the polymer ultra-structure. This is possible because the generation of micromodels ensures that all of them are uncorrelated and they can be combined to cover the surface previously parceled.

The results presented in this work represent a leap forward in the comprehension of the molecular organization on polymer coatings, because they provide a molecular description of structures that previously had to be inferred from visualization techniques that did not reach the atomistic scale. Moreover, it provides a new path to systematically study and comprehend the molecular basis of the functionalities of those coatings that generally are discovered after a new polymeric surface is developed. Using our divide and conquer approach is possible to envisage in a close future the development fine new applications of polymer coating based on specific modifications on the interface of the surface. On that region, any molecular description of an unmodified polymer can be changed *in silico* and then tested within a time frame not yet available through computational brute force.

Acknowledgements

This work was supported by MICINN and FEDER funds (Grant MAT2015-69367-R). Carlos Alemán acknowledges the "ICREA Academia 2015" award for excellence in research, funded by the Generalitat de Catalunya. The authors are in debt with architect

Marta Companys Taxés for the artistic contribution to the elaboration of the graphical abstract.

Supplemental files available: Figures S1-S3, thickness measurements. Table S1, Thickness averages. Figures S4-S9, profilometry measurements. Table S2 Roughness averages.

REFERENCES

1. Li, D.; Zheng, Q.I.; Wang, Y.; Chen H., Combining surface topography with polymer chemistry: exploring new interfacial biological phenomena *Chen Polym. Chem.* **2014**, 5, 14-24.

2. Tretyakov, N.; Müller, M. Directed transport of polymer drops on vibrating superhydrophobic substrates: a molecular dynamics study, *Soft Matter* **2014**, *10*, 4373-4386.

3. Yin, J.; Yagüe, J.L.; Boyce, M.C.; Gleason, K.K. Biaxially mechanical tuning of 2-D reversible and irreversible surface topologies through simultaneous and sequential wrinkling *ACS Appl. Mater. Interfaces 6*, **2014**, 2850-2857.

4. Long, Y.Z.; Li, M.M.; Gu, C.Z.; Wan, M.X.; Duvail, J.L.; Liu, Z.W.; Fan, Z.Y. Recent advances in synthesis, physical properties and applications of conducting polymer nanotubes and nanofibers *Prog. Polym. Sci.* **2011**, *36*, 1415-1442.

5. del Valle, L.J.; Estrany, F.; Armelin, E.; Oliver, R.; Alemán, C. Cellular adhesion, proliferation and viability on conducting polymer substrates *Macromol. Biosci.* **2008**, *8*, 1144-1151.

6. Groenendaal, L.B.; Jonas, F.; Freitag, D.; Pielartzik, H.; Reynolds, J.R. Poly(3,4-ethylenedioxythiophene) and Its Derivatives: Past, Present, and Future *Adv. Mater.* **2000**, *12*, 481-494.

7. Kirchmeyer, S.; Reuter, K.J. Scientific importance, properties and growing applications of poly(3,4-ethylenedioxythiophene) *J. Mater. Chem.* **2005**, *15* 2077-2088.

8. Tamburri, E.; Orlanducci, S.; Toschi, F.; Terranova, M.L.; Passeri, D. Growth mechanisms, morphology, and electroactivity of PEDOT layers produced by electrochemical routes in aqueous medium *Synth. Met.* **2009**, *159*, 406-414.

9. Aradilla, D.; Estrany, F.; Aleman, C. Symmetric supercapacitors based on multilayers of conducting polymers *J. Phys. Chem. C.* **2011**, *115*, 8430-8438.

10. Aradilla, D.; Azambuja, D; Estrany, F.; Casas, M.T.; Ferreira, C.A.; Alemán, C. All-polythiophene rechargeable batteries *J. Mater. Chem.* **2012**, *22*, 13110-13122.

11. Xuan, Y.; Sandberg, M.; Berggren, M.; Crispin, X. An all-polymer-air PEDOT battery *Org. Electron.* **2012**, *13*, 632-637.

12. Aradilla, D.: Pérez-Madrigal, M.M.; Estrany, F.; Azambuja, D.; Iribarren, J.I.; Alemán, C. Nanometric ultracapacitors fabricated using multilayer of conducting polymers on self-assembled octanethiol monolayers *Org. Electron.* **2013**, *14*, 1483-1495.

13. Aradilla, D.; Estrany, F.; Alemán,C. Synergy of the I-/I3-redox pair in the capacitive properties of nanometric poly (3,4-ethylenedioxythiophene) *Org. Electron*. **2013**, 14, 131-142.

14. Aradilla, D.; Estrany, F.; Armelin, E.; Alemán, C. Ultraporous poly (3,4-ethylenedioxythiophene) for nanometric electrochemical supercapacitor *Thin Solid Films* **2012**, 520, 4402-4409.

15. Aradilla, D.; Estrany, F.; Casellas, F.; Iribarren, J.I.; Alemán, C. All-polythiophene rechargeable batteries *Org. Electron.* **2014**, *15*, 40-46.

16. Zanuy, D.; Aleman, C. Resolving the subnanometric structure of ultrathin films of poly (3, 4-ethylenedioxythiophene) on steel surfaces: a molecular modeling approach *Soft Matter* **2013**, 9, 11634-11644.

17. Ahumada, O.; Pérez-Madrigal, M.M.; Ramirez, J.; Curcó, D.; Esteves, C.; Salvador-Matar, A.; Luongo, G.; Armelin, E.; Puiggalí, J.; Alemán, C. Sensitive thermal transitions of nanoscale polymer samples using the bimetallic effect: Application to ultra-thin polythiophene *Rev. Sci. Instrum.* **2013**, *84*, 053904/1-8.

18. Torras, J.; Zanuy, D.; Bertran, O.; Alemán, C.; Puiggalí, J.; Turón, P.; Revilla-López, G. Close contacts at the interface: Experimental-computational synergies for solving complexity problems *Phys. Sci. Rev.* **2018**, *3*, 20170135.

19. Teixeira-Dias, B.; Zanuy, D.; del Valle, J.L.; Estrany, F.; Armelin, E.; Alemán, C. Influence of the Doping Level on the Interactions between Poly (3,4-ethylenedioxythiophene) and Plasmid DNA *Macromol. Chem. Phys.* **2010**, *211*, 1117-1126.

20. Curco, D.; Zanuy, D.; Nussinov, R.; Aleman, C. A simulation strategy for the atomistic modeling of flexible molecules covalently tethered to rigid surfaces: application to peptides *J. Comput. Chem.* **2011**, *32*, 607-619.

21. Duan, Y.: Wu, C.; Chowdhury, S.; Lee, M.C.; Xiong, G.; Zhang, W.; Yang, R.; Cieplak, P.; Luo, R.; Lee, T.; Caldwell, J.; Wang, J.; Kollman, P. A point-charge force field for molecular mechanics simulations of proteins based on condensed-phase quantum mechanical calculations *J. Comput. Chem.* **2003**, *24*, 1999-2012.

22. Preat, J.; Zanuy, D.; Perpete, E.A.; Aleman, C. Binding of cationic conjugated polymers to DNA: atomistic simulations of adducts involving the dickerson's dodecamer *Biomacromolecules* **2011**, *12*, 1298–1304.

23. Baaden, M.; Burgard, M.; Boehme, C.; Wipff, G. Lanthanide cation binding to a phosphoryl-calix[4]arene:the importance of solvent and counterions investigated by molecular dynamics and quantum mechanical simulations *Phys. Chem. Chem. Phys.* **2001**, *3*, 1317-1322.

24. Toukmaji, A.; Sagui, C.; Board, J.; Darden, T. Efficient particle-mesh Ewald based approach to fixed and induced dipolar interactions *J. Chem. Phys.* **2000**, *113*, 10913-10927.

25. Phillips, J.C.; Braun, R.; Wang, W.; Gumbart, J.: Tajkhorshid, E.; Villa, E.; Chipot, C.; Skeel, R.D.; Kale, L.; Schulten, K. Scalable molecular dynamics with NAMD *J. Comput. Chem.* **2005**, *26*, 1781-1802.

26. Berendsen, H.J.C.; Postma, J.P.M.; van Gunsteren, W.F.; DiNola, A.; Haak, J.R. Molecular dynamics with coupling to an external bath *J. Chem. Phys.* **1984**, *81*, 3684-3690.

27. Martyna, G.J.; Tobias, D.L.; Klein, M.L. Constant pressure molecular dynamics algorithms *J. Chem. Phys.* **1994**, *101*, 4177-4189.

28. Feller, S.E.; Zhang, Y.; Pastor, E.W.; Brooks, B.R. Constant pressure molecular dynamics simulation: The Langevin piston method *J. Chem. Phys.* **1995**, *103*, 4613-4622.

29. Toxvaerd, S. Molecular dynamics calculation of the equation of state of alkanes *J. Chem. Phys.* **1990**, *93*, 4290-4295.

30. Wennberg, C.L.; Murtola, T.; Hess, B.; Lindahl, E. Lennard-Jones lattice summation in bilayer simulations has critical effects on surface tension and lipid properties *J. Chem. Theory Comput.* **2013**, *9*, 3527-3537.

31. Gadelmawla, E.S.; Koura, M.M.; Maksoud, T.M.A.; Elewa, I.M.; Soliman, H.H. Roughness parameters *J. Mater. Process. Tech.* **2002**, *123*, 133-145.

32. Maione, S.; Fabregat, G.; del Valle, L.J.; Ballano, G.; Cativiela, C.; Alemán, C. Electro-biocompatibility of conjugates designed by chemical similarity *J. Pept. Sci.* **2014**, *20*, 537–546.

33. Heinz, H.; Ramezani-Dakhel, H. Simulations of inorganic–bioorganic interfaces to discover new materials: insights, comparisons to experiment, challenges, and opportunities *Chem. Soc. Rev.* **2016**, *45*, 412- 448.

34. Janke,W.; Paul, W. Thermodynamics and structure of macromolecules from flat-histogram Monte Carlo simulations *Soft Matter* **2016***, 12*, 642- 657.

35. Martin, D.C.; Wu, J.; Shaw, C.M.; King, Z.; Spanninga, S.A.; Richardson-Burns, S.; Hendricks, J.; Yang J. The Morphology of Poly(3,4-Ethylenedioxythiophene), *Polym. Rev.* **2010**, *50*, 340-384.

36. Ocampo, C.: Oliver, R.; Armelin, E.; Aleman, C.; Estrany, F. Electrochemical synthesis of poly (3,4-ethylenedioxythiophene) on steel electrodes: properties and characterization *J. Polym. Res.* **2006**, *13*, 193–200.

37. Niu, L; Kvarnstrom C.; Froberg, K.; Ivaska, A. Electrochemically controlled surface morphology and crystallinity in poly(3,4-ethylenedioxythiophene) films *Synthetic Metals* **2001**, *122,* 425–429.

CAPTIONS TO FIGURES

Figure 1.- 2D Height AFM images of: **(a)** PEDOT at θ= 1s and **(b)** at θ= 3s. 3D topographic AFM images of: **(c)** PEDOT at θ= 1s and **(d)** at θ= 3s.

Figure 2.- Flow chart of the methodological approach presented in this work. ***Top panel****: from left to right*, an independent rigid micromodel (generated using stochastic methods) and its relaxed form (after a short trajectory of Molecular Dynamics). ***Middle panel:*** lateral association of 26 independent micromodels into a 200 nm surface segment (see text why 26 segments are used). ***Bottom panel*****:** lateral association of 260 micromodels into a 2μm surface segment. Each change of order of magnitude is remarked by framing the smallest atomistic model that would lead to a larger system by merging several of those small partitions.

Figure 3.- (a) Accumulated radial distribution function of all inter chain EDOT–EDOT distances, measured from the centers of mass, for the 6 built macromodels. Dashed red lines indicate experimentally detected distances characteristic of highly crystalline PEDOT films deposited on steel (reference 36) **(b)** Height topographic profiles obtained from AFM images of deposited PEDOT after 1s of electropolymerization. **(c)** Height profile obtained from each generated macromodel. In both panels *(a)* and *(c)*, each colored line corresponds to a single macromodel.

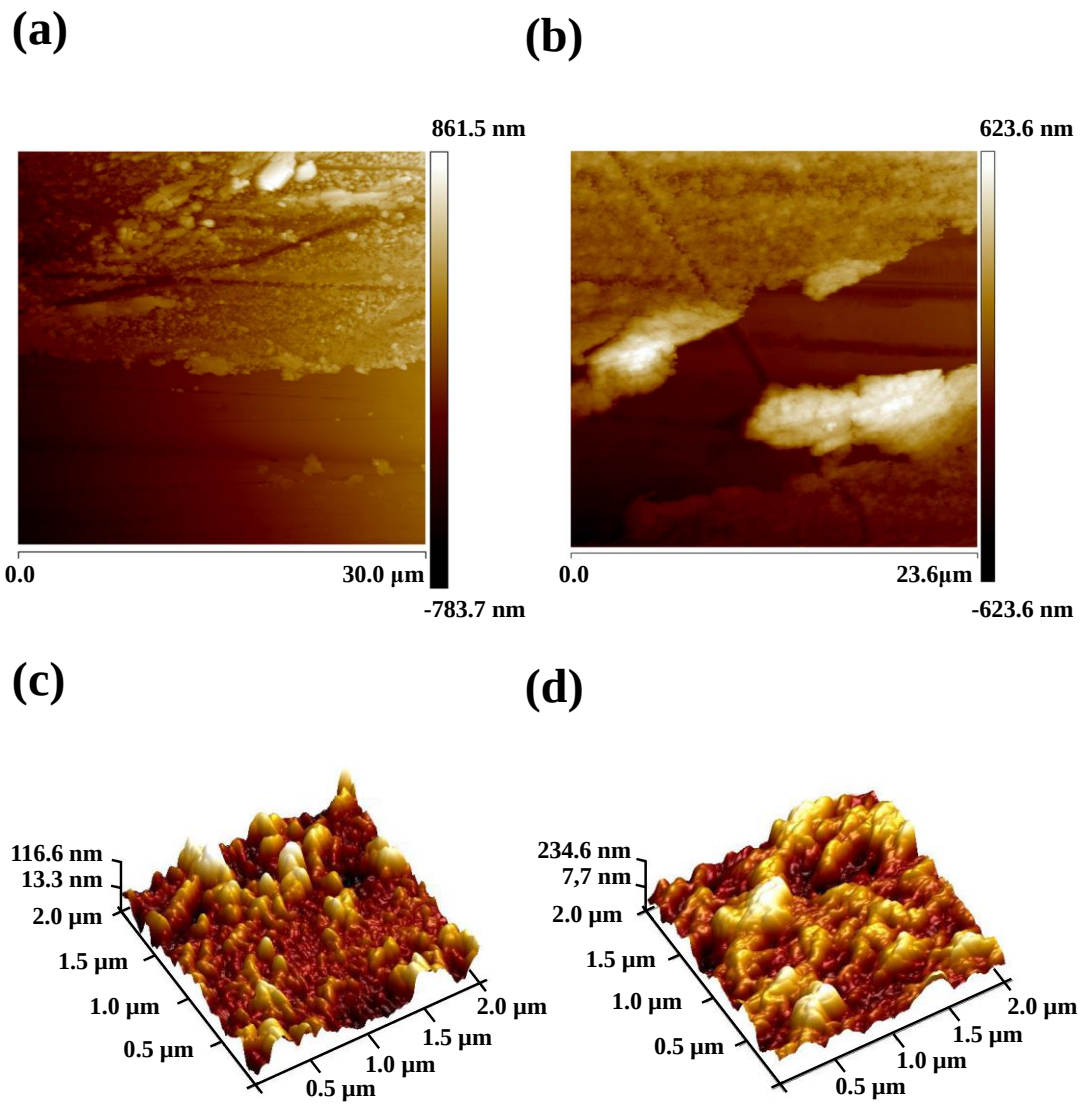
(a)
(b)
861.5 nm
-783.7 nm
0.0
30.0 µm
623.6 nm
-623.6 nm
0.0
23.6µm
(c)
(d)
116.6 nm
13.3 nm
2.0 µm
1.5 µm
1.0 µm
0.5 µm
2.0 µm
1.5 µm
1.0 µm
0.5 µm
234.6 nm
7,7 nm
2.0 µm
1.5 µm
1.0 µm
0.5 µm
2.0 µm
1.5 µm
1.0 µm
0.5 µm

Figure 1

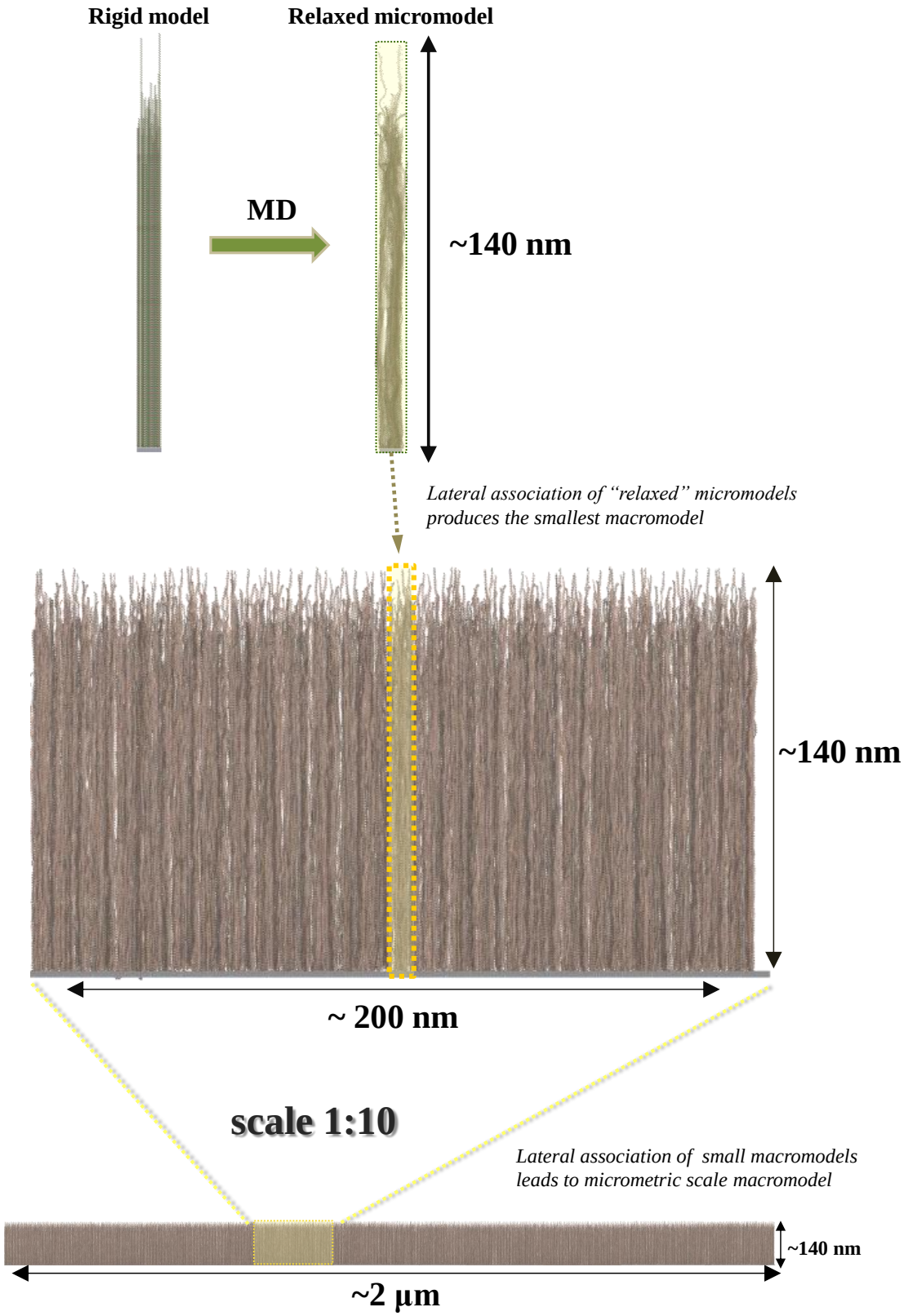
Rigid model
Relaxed micromodel
MD
~140 nm
Lateral association of "relaxed" micromodels
produces the smallest macromodel
~140 nm
~ 200 nm
scale 1:10
Lateral association of small macromodels
leads to micrometric scale macromodel
~140 nm
~2 µm

Figure 2

(a)

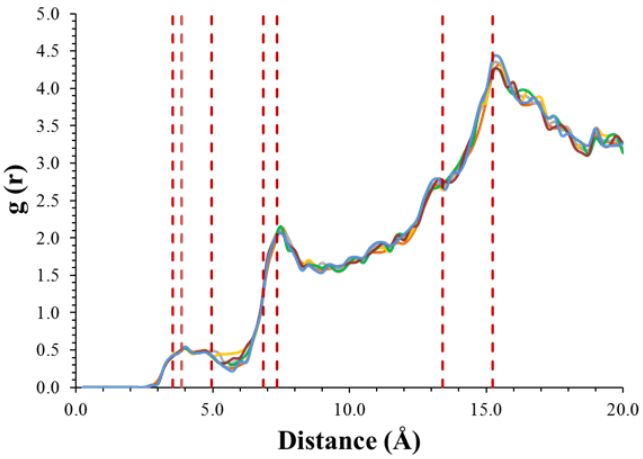
g (r)
Distance (Å)

(b)

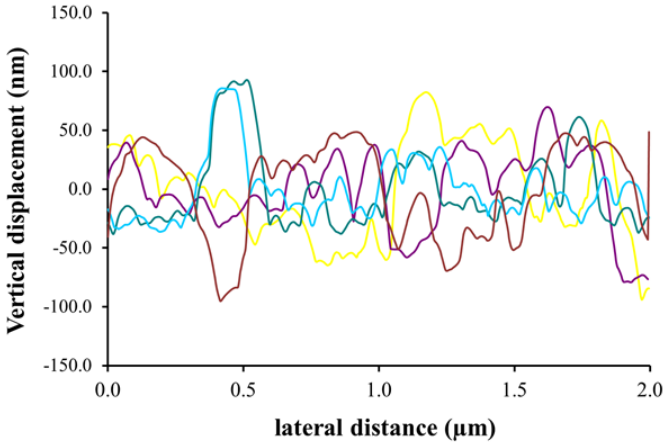
Vertical displacement (nm)
lateral distance (µm)

(c)

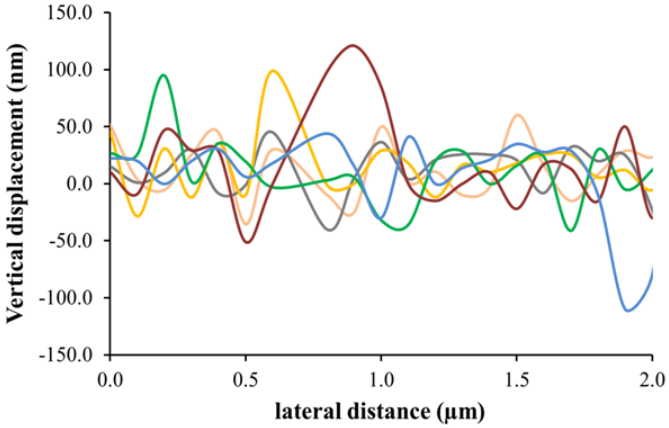
Vertical displacement (nm)
lateral distance (µm)

Figure 3

TOC